1999-09

Adjustment of the Summer Marine Boundary Layer around Point Sur, California

Dorman, C.E.; Rogers, D.P.; Nuss, W.; Thompson, W.T.

American Meteorological Society

Adjustment of the Summer Marine Boundary Layer around Point Sur, California

C. E. DORMAN

Coastal Studies, Scripps Institution of Oceanography, San Diego, California

D. P. ROGERS

Physical Oceanography Research Division, Scripps Institution of Oceanography, San Diego, California

W. NUSS

Meteorology Department, Naval Postgraduate School, Monterey, California

W. T. THOMPSON

Marine Meteorology Division, Naval Research Laboratory, Monterey, California

ABSTRACT

An instrumented C-130 aircraft flew over water around Point Sur, California, on 17 June 1996 under strong northwest wind conditions and a strong marine inversion. Patterns were flown from 30- to 1200-m elevation and up to 120 km offshore. Nearshore, marine air accelerated past Point Sur, reaching a surface maximum of 17 m s^{-1} in the lee. Winds measured over water in and above the marine layer were alongshore with no significant cross-shore flow. Sea level pressure, 10-m air temperature, and air temperature inversion base generally decreased toward the coast and were an absolute minimum just downcoast of the wind speed maximum. The sea surface temperature also decreased toward the coast, but was an absolute minimum directly off Point Sur. The near-coast, air temperature inversion base height was 400 m north of Point Sur, decreased to a minimum of 50 m in the lee of Point Sur, then increased farther to the south. Wind speeds were at a maximum centered along the air temperature inversion base; the fastest was 27 m s^{-1} in the lee of Point Sur.

Using a Froude number calculation that includes the lower half of the capping layer, the marine layer in the area is determined to have been supercritical. Most of the marine layer had Froude numbers between 1.0 and 2.0 with the extreme range of 0.8–2.8. Temperatures in the air temperature inversion in the lee were substantially greater than elsewhere, modifying the surface pressure gradient. The overall structure was a hydraulic supercritical expansion fan in the lee of Point Sur under the influence of rotation and surface friction.

The Naval Research Laboratory nonhydrostatic Coupled Ocean/Atmosphere Mesoscale Prediction System (COAMPS) indicated a broad, supercritical marine boundary layer moving to the south along central California and Point Sur during the aircraft flight. The marine boundary layer thinned and accelerated into the lee of Point Sur, which was the site of the fastest sea level wind speed along central California. Isotherms dip and speeds decreased in the lee of Point Sur in the capping inversion well above the marine layer. COAMPS forecasted a compression shock wave initiating off the upwind side of the topography behind Point Sur and other coastal points to the north. Evidence from the model and the aircraft supports the existence of an oblique hydraulic jump on the north side of Point Sur.

1. Introduction

The low-level coastal winds along the U.S. west coast have been studied for some time on account of their implications to a range of applied and theoretical interests. One of the first complete coastal descriptions of

Corresponding author address: Dr. Clive E. Dorman, Coastal Studies, Scripps Institution of Oceanography, University of California, San Diego, La Jolla, CA 92093-0209.
E-mail: clive@coast.ucsd.edu

the West Coast wind field was based upon ship observations (Nelson 1977). This analysis showed that part of the westerly, low-level airflow turns south as it approaches the Oregon–British Columbia coast. Along southern Oregon and central California this becomes a broad, alongshore, summer wind maxima. Using coastal buoy observations, Dorman and Winant (1995) found two locations where there are peaks in the monthly mean, alongcoast winds. One occurs in northern California near Bodega Bay and the other near Point Conception to the south.

Small-scale variation in the winds near Point Arena

during the Coastal Ocean Dynamics Experiment (CODE) was explained as a supercritical marine boundary layer passing Point Arena, accelerating and thinning in an expansion fan in the lee, followed by a slowing and thickening in a hydraulic jump (Winant et al. 1988). This behavior in the winds depends in part upon the presence of a strong summer subsidence inversion capping a cool moist marine layer that often exceeds 10°C in strength (Neiburger et al. 1961). The inversion base surface tilts downward to the east, with a typical 300–400-m elevation at the coast, although values can range from less than 100 m to more than 800 m (Beardsley et al. 1987; Dorman 1985, 1987). This indicates that similar behavior may occur on a frequent basis near other coastal points and capes along the California coast. Winant et al. (1988) suggested that supercritical marine boundary layer flow was a common occurrence on the midlatitude west coasts of all continents. However, the applicability of this explanation to variations in wind speeds around other coastal prominences has not been documented. In addition to the generality of the occurrence of supercritical features, the seaward extent of the supercritical features is uncertain as the aircraft mapping during CODE was limited to the inner 30 km of a 100-km stretch of the coast.

Simple numerical models have been able to replicate these hydraulic flow effects as shown by Samelson (1992), who found that a hydraulic supercritical model including rotation and friction was a substantial improvement over a frictionless model. It explained why there was a maximum in speed at the coast with a layer depth minimum a little downwind of a topographic bend in a coast. As a result, the expansion fan wind speeds, surface pressure, and layer depth form circular contours in the lee of the point rather than straight lines radiating outward in a fan-shaped pattern from the topographic bend as predicted by the nonrotational, inviscid hydraulic model. These results are encouraging: the basic dynamic processes as modeled in simplified models can produce the qualitatively correct solution.

In spite of the theoretical and model developments, only the limited area around Point Arena has had aircraft sampling over water to measure supercritical flow. It is uncertain how representative this might be of the west coast of the United States. To follow up on the nature of the coastal wind field, a series of long-range, instrumented aircraft flights were made along the Oregon and California coast in June 1996. A broad zone of high-speed winds under a low inversion were found along Point Sur, California, suggesting that this may be a supercritical flow field adjusting to the topography and further accelerating in the lee of Point Sur. By presenting the details of one of these flights in the context of the other observations, the object of this paper is to shed light on the structure of the marine boundary layer in the vicinity of Point Sur. In addition, numerical model simulations with the navy's Coupled Ocean/Atmospheric Mesoscale Prediction System (COAMPS) were done in real time as well as retrospectively to provide a larger-scale context of the marine boundary layer structure for the aircraft and to test the ability of this operational model to produce correct mesoscale structure in the winds near Point Sur.

2. The measurements and the model

The majority of the data shown here were taken with the National Center for Atmospheric Research (NCAR) Hercules EC-130Q aircraft. This is a high-wing, four-engine, turboprop aircraft. It has a nominal airspeed of 100 m s^{-1} and a 10-h endurance. A Global Positioning System, an inertial navigation system, and a radar altimeter ensure accurate location and resolution of the aircraft movement. An extensive atmospheric measurement system includes observations of winds, pressure, air temperature, and moisture as well as radiometric surface temperature to obtain the sea surface skin temperature, called the SST. Signals from all sensors are simultaneously sampled at 10 kHz. Analog signals are sampled at 5 kHz with filtering and other processing to eliminate aliasing. An onboard Sun SPARC-10 computer system samples, records, and displays the data. All sensor data used in this paper were decimated and converted to 1 Hz.

The C-130 made five flights in strong northerly winds in the vicinity of Point Sur in June 1996. All of the aircraft data presented here come from a flight on 17 June that began in the area near 1800 UTC and ended at 0100 UTC 18 June. A series of level traverses at 30 m, approximately 200 m, 800 m, and a sawtooth pattern that extended from 30 m to above 800 m elevation were flown in both alongcoast and cross-coast legs. A nominally 30-m level flight leg will be referred to as a 10-m track when pressure and air temperature are systematically adjusted to 10 m as explained in section 4. Vertical section profiles were constructed from the various levels flown along a leg and the sawtooth soundings.

In addition to standard flight-level observations, the C-130 also carried a Scanning Aerosol Backscatter Lidar (SABL) developed for the NCAR Remote Sensing Facility. SABL is a dual-wavelength lidar operating with 75 mJ at 1064 nm (red) and 50 mJ at 532 nm (green). Background filter bandwidths are 0.92 nm at 1064 nm and 0.16 nm at 532 nm. The lidar beam was continuously operated either pointed upward or downward.

The Naval Research Laboratory nonhydrostatic COAMPS was run in real time in support of the observational program and provides a context for the aircraft flights. COAMPS consists of a three-dimensional, fully compressible, nonhydrostatic mesoscale atmospheric model and a hydrostatic ocean model (not used in the present study) as described by Hodur (1997). The domain configuration used in support of the operational program consisted of three horizontally nested grids oriented parallel to the California coast with resolutions of 81, 27, and 9 km, respectively. The 9-km domain will
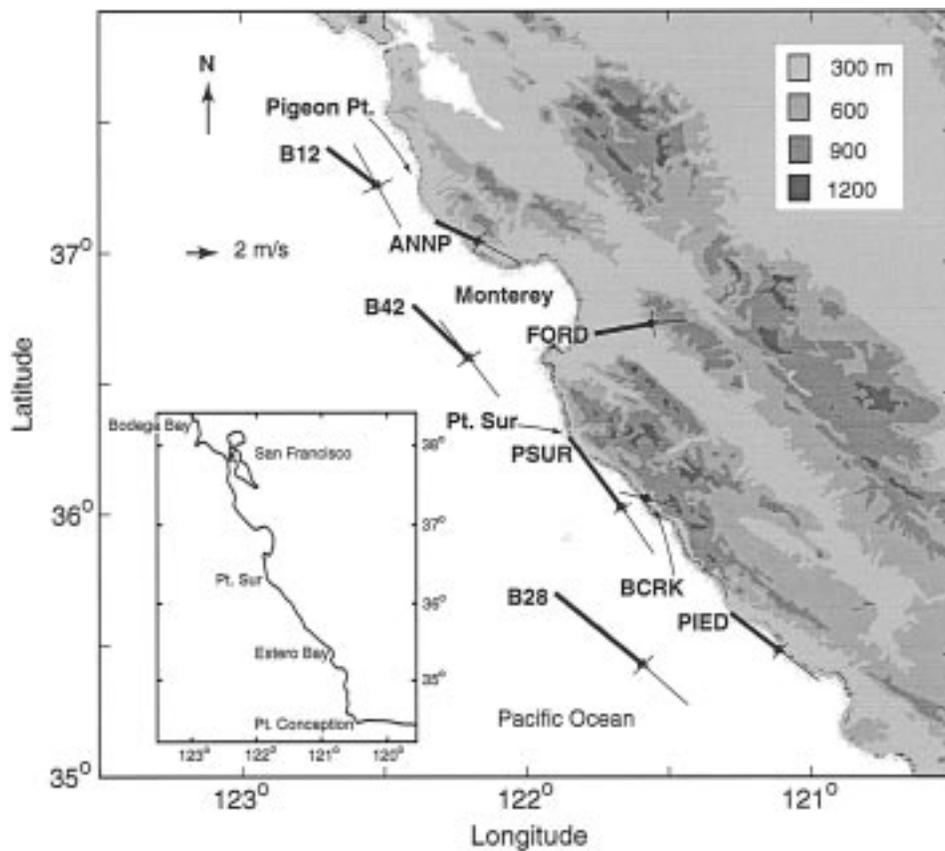
FIG. 1. Topography and mean surface winds for 10 Jun–10 Jul 1996. The coastal topography extends well above the marine layer. Coastal northerly surface winds accelerate to a maximum in the lee of Point Sur, then slow somewhat to PIED. In contrast, the winds are very weak at BCRK.

be shown in section 6. The model depth extended to 30 km with vertical resolution ranging from 20 m near the surface to 7.5 km near the top. This model was run in a continuous data assimilation mode during the month of June 1996. Thus, the assimilation cycle had run for 16 days prior to the period of interest. The data assimilation procedure involved using a previous model 12-h forecast as the first guess in an optimum interpolation analysis of the current observational data. The analysis

was performed on each of the three nests. Model products are shown in section 6.

3. Mean structure and synoptic setting

The mean overwater winds for 10 June–10 July 1996 shown in Fig. 1 and Table 1 indicate the tendency of the flow to interact with the elevated topography, which forms a solid coastal barrier below 800 m along most

TABLE 1. Surface station statistics for 10 Jun 1996–10 Jul 1996.

|		Speed (m s^{-1})				Air temperature (°C)			Pressure (hPA)
		Mean	Std maj	Std min	Range*	Mean	Std	Range*	range*
B12	Buoy 12	4.6	3.6	1.2	0.1	11.8	0.7	0.7	1.4
B42	Buoy 42	5.7	3.6	1.0	0.7	14.2	0.7	0.5	1.2
B28	Buoy 28	8.3	4.4	1.0	0.7	12.2	0.8	0.9	1.5
ANNP	Año Nuevo	3.5	3.2	0.9	3.5	12.5	1.9	4.1	0.9
FORD	Ford Ord	4.2	2.4	1.0	5.5	12.7	3.0	5.6	M
PSUR	Pt. Sur	6.6	4.1	0.7	1.6	12.6	1.6	3.7	0.8
BCRK	Big Creek	0.6	2.1	0.5	2.7	12.4	1.7	2.6	1.2
PPED	Pt. Piedras Blancas	4.5	3.6	0.8	4.1	11.8	1.1	1.9	0.3

* Range is absolute change between 1200 and 0000 UTC.
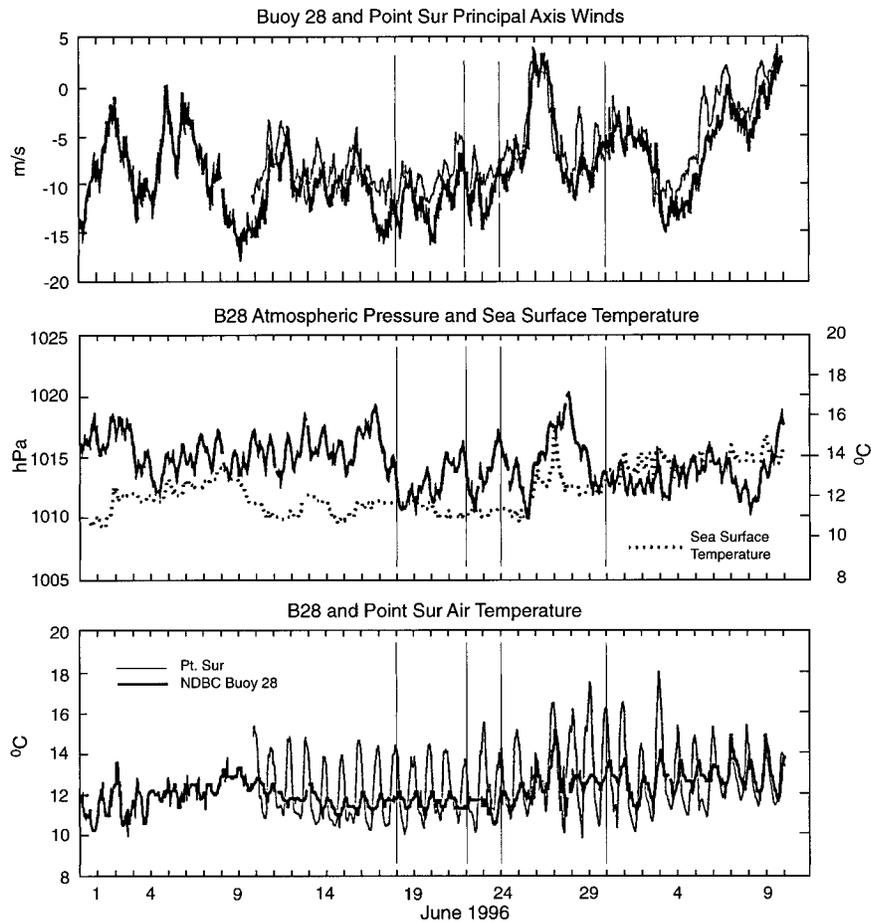
Fig. 2. June time series for PSUR (light) and B28 (dark). Wind speeds were strong (13–15 m s^{-1}) at buoy 28 during the 17 Jun C-130 flight. Point Sur aircraft flights are noted by vertical lines.

of the coast in our area of study. The climatological coastal northerly wind accelerates past Año Nuevo (ANNP) and then decelerates by Point Piedras Blancas (PIED) in the southern end of the figure. Some of the northerly flow divides around the topography south of Monterey and turns to the east into the gap at the mouth of the southward extending Salinas River Valley, and another gap that exists on the extreme eastern end of the Monterey Bay. Farther south along the coast, the winds at Big Creek (BCRK) are very weak in the lee of Point Sur, which is confirmed by local observers.

Temporal trends are reflected in the time series of surface variables shown in Fig. 2 for the Point Sur coastal station and National Data Buoy Center buoy 46028 (B28), around the time of the aircraft flights. The 17 July flight was during a period of continuing strong northerly winds. Diurnally, wind speeds at B28 are fastest at 0300–0400 UTC and slowest at 1500–2000 UTC.

Mean daily temperatures at B28 had modest trends, remaining between 11° and 15°C for the entire period (Fig. 2), which is characteristic of its marine location and weak, midlevel synoptic forcing during this time of

year. The sea surface temperature was about 1°C cooler than the air and without trend over 10–26 June. Diurnal variations of air temperatures at Point Sur (PSUR) were 4°C, whereas it was only 1°C at B28.

Typical of the climatological pattern during June, high pressure predominated offshore with lower pressure over the continent (not shown). The synoptic conditions for 17 June 1996 were consistent with the weak signal in the time series (Fig. 2) and were characterized by the eastward movement of a weak upper-level trough across northern California and an associated amplification of the subtropical surface high pressure to the north and west of California. A strengthening high pressure system, coupled with strong diurnal pressure falls over the land area during the day, resulted in a strong sea level pressure gradient across California by 0000 UTC 18 June, which supposed 10–13 m s^{-1} northwesterly surface winds along the coast. Observations from the Naval Postgraduate School (NPS) profiler at Fort Ord show a dramatic shallowing of the marine boundary layer during the period (from 700 to 300 m),
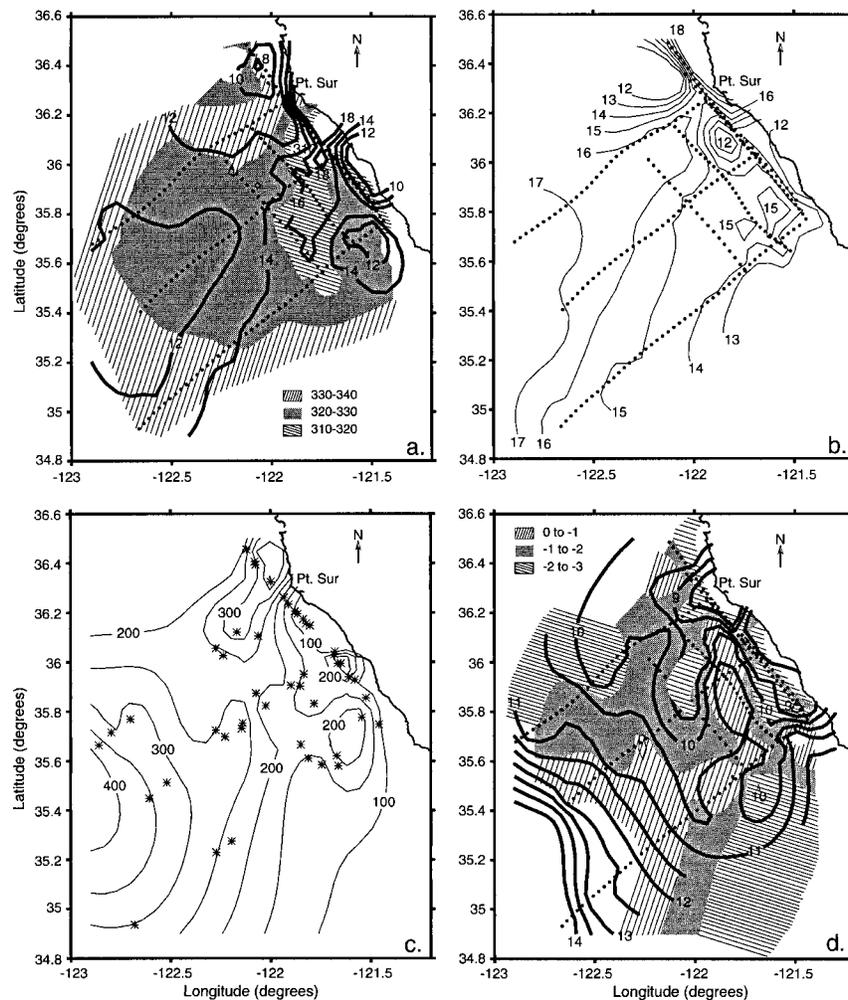
FIG. 3. Near–sea surface aircraft maps. Dots are the decimated data points used for the analysis and show flight tracks: (a) 10-m wind speed (solid lines, m s^{-1}) and direction (hatched and shaded, °) and (b) 10-m pressure minus 1000 (hPa). (c) Air temperature inversion base height (m) based upon aircraft soundings taken at asterisks. (d) Sea surface temperature (solid lines, °C) and sea surface temperature minus 10-m air temperature (hatched and shaded, °C).

which is consistent with the passage of an upper-level trough and increased subsidence after trough passage.

4. Observed structure

a. Horizontal structure

To document the horizontal structure of the lower atmosphere, surface maps were constructed from the nominal 30-m elevation tracks by adjusting measurements to a common 10-m elevation so as to be directly comparable with fixed station measurements. The wind speeds were corrected to 10 m, assuming a log-wind law relationship where the drag coefficient is a function of the final wind speed (Large and Pond 1981; technique described in Dorman and Winant 1995). Pressure was corrected to sea level using hydrostatics and the aircraft potential temperature to compute the air density. Finally,

the B28 pressure average was computed for the entire time of the aircraft flight on 17 June and the difference between the aircraft-corrected buoy mean and the values directly measured on the buoy was also subtracted from the aircraft sea level pressure. This was done to adjust the aircraft pressure for the variation over the flight, which amounted to about 2 hPa. The air temperature was corrected to 10 m assuming neutral stability and an adiabatic lapse rate. The sea surface temperature estimate was corrected for sky reflection and nonblackness of the sea surface radiation in the infrared (Paulson and Simpson 1981; Hignett 1997, personal communication). No changes were made in the wind direction.

The low-level winds exhibited the greatest amount of structure within about 30–40 km off the coast with much more uniform speed and direction found farther off-shore. Figure 3a shows the low-level wind direction to

be from 320° to 330° distant from the north side of Point Sur and beyond 30 km off the coast to the southwest of Point Sur, which is consistent with the synoptic-scale pressure gradient and analyzed winds. Wind speeds of 12–14 m s^{-1} characterized the flow in the offshore area. Closer inshore both north and south of Point Sur, the wind direction and speed exhibited more variation, with the direction primarily conforming to the local coastal orientation. Inshore, the winds were a maximum of 18 m s^{-1} to the south of Point Sur.

The sea level pressure distribution derived from the aircraft (Fig. 3b) is in general agreement with the synoptical-scale pressure analysis that has a general decrease in pressure toward the inshore and to the south. However, the aircraft-observered pressures show considerable mesoscale structure along the coast, where the pressure minimum of 1012 hPa was in the lee of Point Sur and coincident with the wind speed maximum.

Outside the near-coastal region, there was a general increase in the inversion base height from about 200 m to about 400 m at the point farthest from the coast sampled by the aircraft (Fig. 3c). Close to the coast and just north of Point Sur was a maxima of 400 m north, coincident with the local sea level pressure maximum and wind changes, that is believed to have been an oblique hydraulic jump, which will be discussed later. An absolute minimum base-height measurement of 57 m was in the lee of Point Sur and close to the coast at 36°N, 121.7°W. This also extends to the south as a height minimum. The inversion base-height topography was coincident with the mesoscale structure in the sea level pressure and 10-m wind speeds.

Another indication of the structure is the potential temperature difference between the top and the base of the air temperature inversion (the inversion strength). The smallest difference is 8 K in the extreme southwest (not shown). This grades toward a coastal maximum of 14–16 K, which is spatially correlated with the lowest inversion base height.

Sea surface temperatures are minimal along the inshore track and are shown in Fig. 3d to have increased by 5°C to the southwestern edge of the measurements. The absolute minimum is 8.5°C just off Point Sur located near but not exactly under the wind speed maximum. The air temperature (not shown) has a range of only about 2°C over the map and is lowest over the inshore track. As a result, the sea minus 10-m air temperature (Fig. 3d) is most extreme near Point Sur (−4°C). The difference decreases to less than +1°C in the most distant offshore southwestern portion of the mapped area.

b. Ten-meter tracks

Finer details of the mesoscale structure in the wind and other fields near the coast are brought out by plotting aircraft time series and lidar observations along a constant flight level leg. Along the alongshore track closest to shore, the 10-m winds enter at the north end at 11 m s^{-1}, increase to 14 m s^{-1}, then suddenly drop to 6 m s^{-1} near 36.45°N (Fig. 4). With the sudden drop, the wind shifts abruptly to more northerly by 30° and the pressure rises by 1 hPa. The case will be made in section 7 that this feature is an oblique hydraulic jump. Continuing to the south along the track, the wind speeds increase while the winds shift to more westerly and the pressure and sea surface temperature fall. These variables all level off between 36.15° and 36.05°N, then reverse trends. Maximum 10-m wind speeds of 19 m s^{-1} are associated with the lowest track pressure of 1012.5 hPa (excluding the dip on the extreme southerly end).

While flying at 1000 m along the coast, on the east track discussed above, the lidar was pointed downward. Shown in Fig. 5 is the green wavelength, but the main structures revealed by this wavelength are duplicated in the red. The main return off the air temperature inversion base varied smoothly with extremes of 100 and 420 m. The grand minimum was coincident with the fastest 10-m wind speeds in the time series (Fig. 12). The rapid rise on the north end (HJ) is coincident with the 10-m wind decrease, direction shift, and pressure rise that are consistent with an oblique hydraulic jump. This is followed by at least five peaks of a 3.5-km wavelength gravity wave.

The structure in the cross-coast direction is illustrated in finer detail in the time series from the middle cross-coast track shown in Fig. 6. Starting from the east, the winds quickly shift from the near-track mean to a maximum of 18 m s^{-1} and a direction of 305° centered at 121.75°W. The wind speed and direction farthest offshore approach 12 m s^{-1} and 330°. In contrast, the pressure and temperatures generally increase along the track toward the west once away from the minimum near the east end. This structure would be consistent with the nearshore, low-level air, being in a quasigeostrophic balance in the cross shore but going downgradient along the shore. Thompson et al. (1997) found this same balance condition when they evaluated terms of the momentum budget at several points along the California coast in an area of northwesterly flow using a numerical model.

While flying at 900 m on the cross-coast track above mentioned, the lidar was pointed downward to detect the air temperature inversion base height (Fig. 7). The inversion base height rises first steeply from a minimum of 100 m in the east, then more slowly to 400 m in the west. This gradual and relatively smooth change in the inversion is consistent with the rather uniform increase in pressure offshore.

Well above the marine boundary layer at 900–1000-m elevation, the winds are almost completely from the north-northwest (Fig. 8). At the extreme easterly, coast-parallel aircraft track line, the direction is the same although the speeds are much weaker. The direction is essentially preserved all the way down through the air
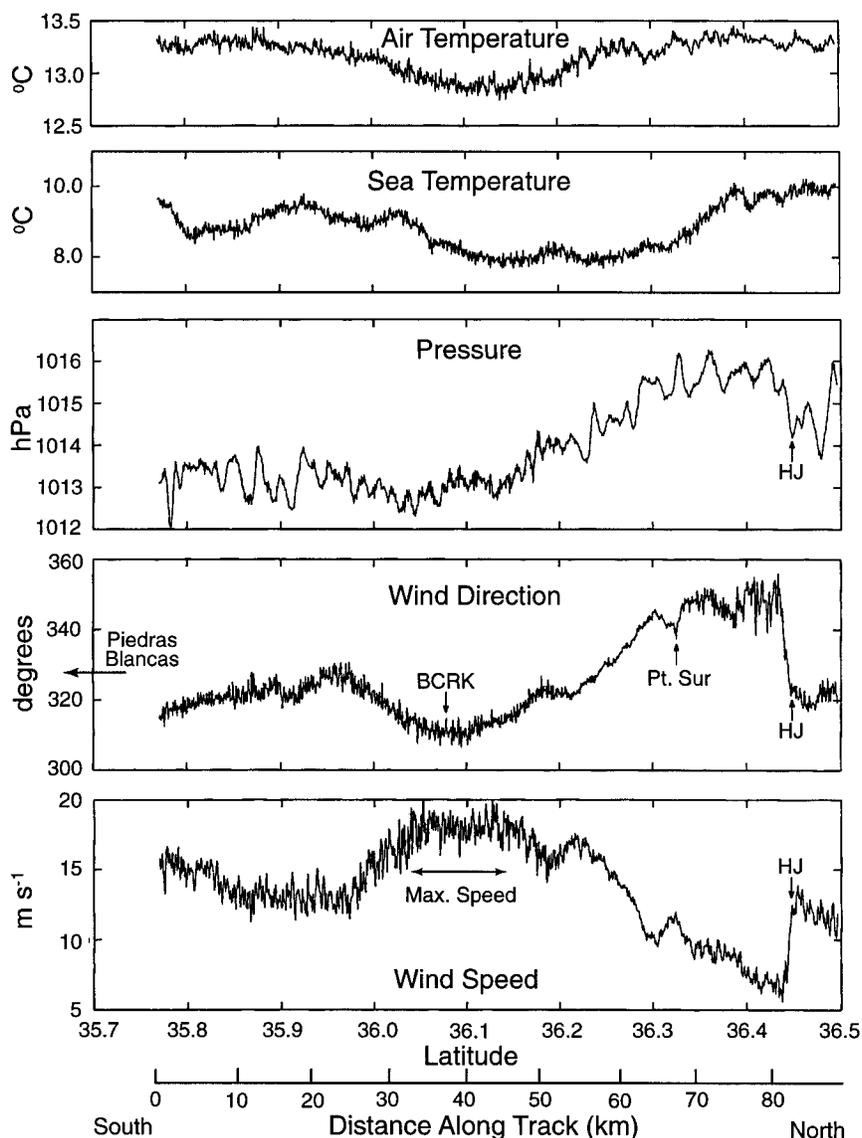
FIG. 4. The 10-m along coast east track 3, 17 Jun. The lowest level for Figs. 5 and 9. There appears to be an oblique hydraulic jump in the north end of the track (HJ) where the speed decreases from 14 to 6 m s^{-1}, the wind shifts 15°, and pressure increases 1 hPa. The center of the wind speed maximum is displaced to the south from the center of the sea surface temperature minimum, but is concurrent with the air temperature minimum.

temperature inversion and the marine layer below (not shown) with little wind direction shear. Thus, there is no sense of significant cross-shore airmass movement below 1000-m elevation over the sea and especially not in the air temperature inversion.

c. Vertical structure

The relationship between the marine boundary layer structure and the winds is highlighted in vertical cross sections along and across the coast (Fig. 9). The along-coast structure near the coast shows the lowest inversion to the south of Point Sur and the fastest wind speeds of 26 m s^{-1} near the base of the air temperature inversion. To the north of this local wind maxima, the wind speed in the core of maximum winds decreases slowly while increasing in elevation to the north end of the track. To the south, the wind speeds in the core of maximum values decreases more quickly but does not change elevation, while the air temperature inversion increases in height. Above the inversion base, there is a secondary maximum of 20 m s^{-1} centered at 400 m and at 80 km along the track just above the south side of the lower-level, absolute maximum. On the north side of the section, at 500 m, is a weaker speed maximum. Both the 400- and 500-m wind speed maxima are in the upper
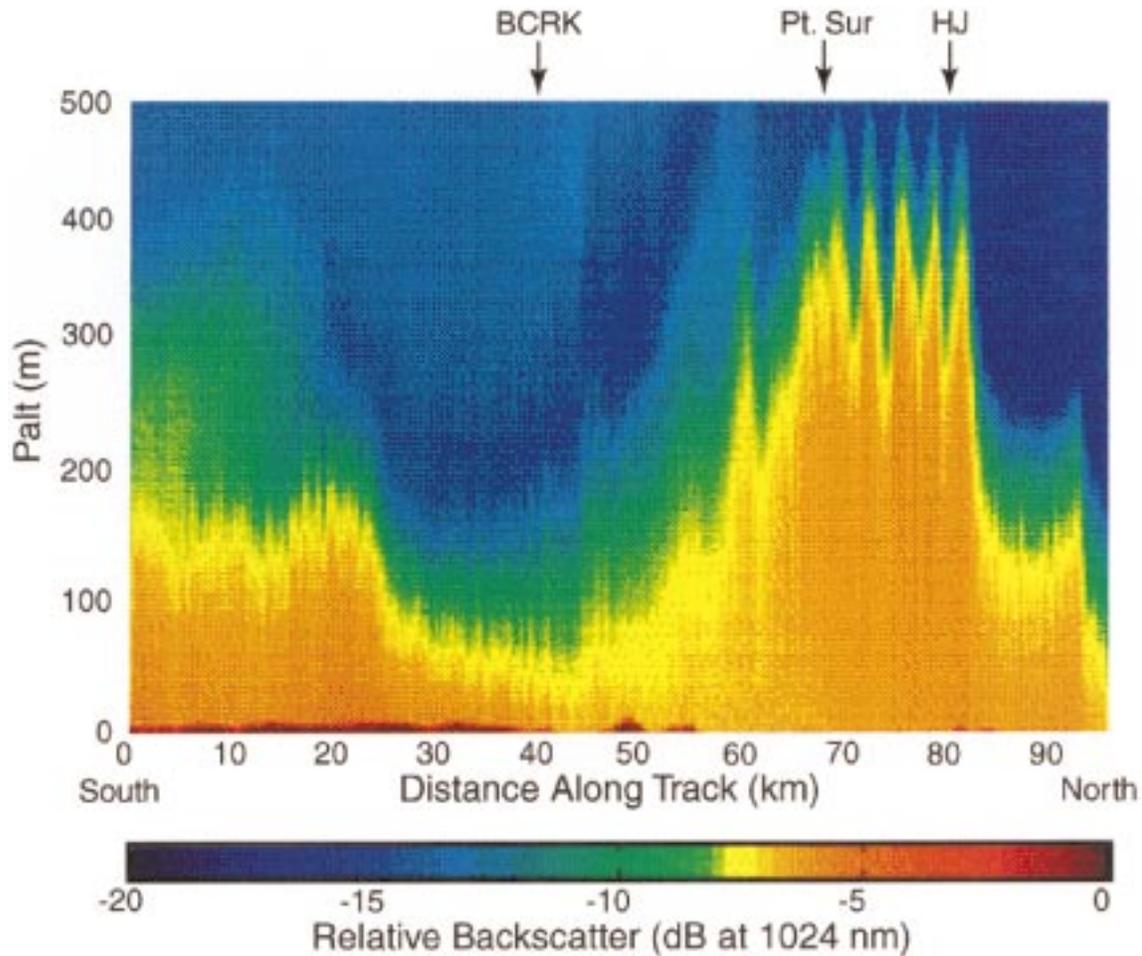
FIG. 5. Green, downward pointed lidar while flying at 1000 m on an alongcoast east track corresponding to Figs. 4 and 9. Main return is from air temperature inversion base that is between 57 m to 500 m above sea level. On north end, HJ marks sharp rise associated with an oblique hydraulic jump, followed by five gravity wave peaks. The minimum in height in the center of the track corresponds to the fastest 10-m winds.

portion of the air temperature inversion and associated with an upward bulge of the isentropes.

Farther offshore, the alongcoast vertical structure is similar to that at the coast except that the features are at higher elevation, and the south end of the section is still within the region of higher velocity surface winds (Fig. 10). The wind speed maximum of 28 m s^{-1} is found at 300-m elevation at 50 km along the track and at the base of the air temperature inversion. The speed in the core of maximum winds decreases to 24 m s^{-1} and lifts along with the inversion base to 420-m elevation at the north end of the section. Above the inversion on the south end of the section (400 m, 60 km), there is only a weak indication of the secondary wind maxima above the inversion that was found closer to the coast (Fig. 9).

The cross-coast sections support the basic relationship between the winds and inversion base height found in the alongcoast sections. In general, the inversion tilts upward in the offshore direction and speeds are a maximum along the air temperature inversion base (Fig. 11).

The maximum speeds decrease slowly in the offshore direction. From the air temperature inversion base to the top of the section, the isentropes and isotachs tilt upward in the offshore direction.

While the general structure shown in Fig. 11 for the mid-cross-coast section is consistent for the other cross-coast sections, several important differences occur. First, the absolute inversion base minimum occurs at or very near the coast for the northern and middle cross sections, while it occurs 40 km offshore for the southern cross section and then rises weakly toward the coast where the surface winds are greatly reduced. Second, the slope of the inversion in the cross-coast direction varies from north to south. The northern section shows only a weakly sloped inversion, while the southern section shows a stronger slope.

d. Temporal changes

While the basic atmospheric structure did not change, there were significant temporal changes in the atmo-
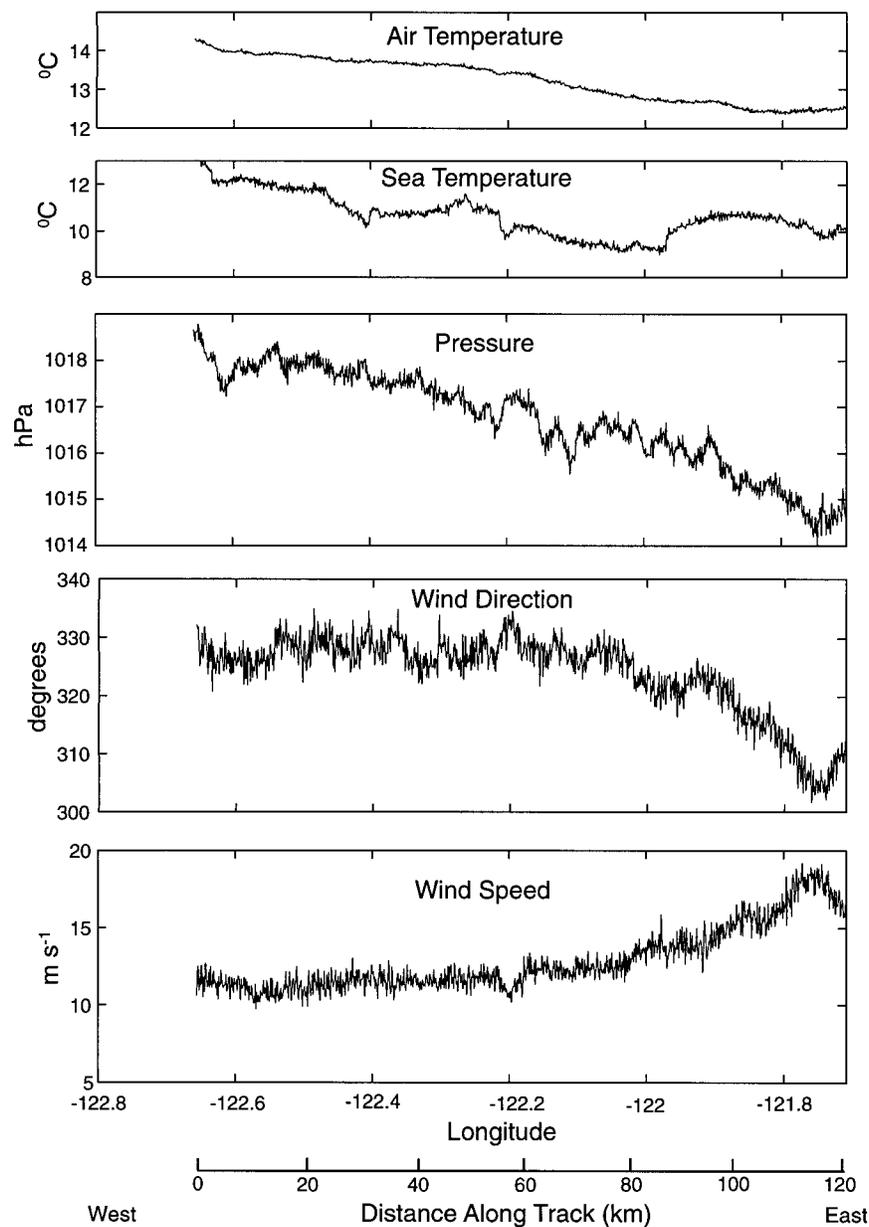
FIG. 6. The 10-m cross-coast midtrack, 17 Jun. The lowest level for Figs. 7 and 11.

sphere during the flight of the aircraft with the greatest occurring closest to the coast. The winds at B28 increased by 25% over the flight time of the aircraft. This was evident from the aircraft's inshore track flight (repeated at the start, middle, and end of the flights) that showed a general speed increase as the day progressed. However, the largest wind speed increases occurred between 36° and 36.3°N with the most extreme change between 36° and 36.1°N, which also resulted in a shift of the absolute maximum 6 km to the south.

To a degree, the vertical profiles reflected some of the changes seen at the surface. Compared to the late afternoon, alongcoast, inshore track (Fig. 9), the marine layer was deeper in the morning (Fig. 12), and there was only a single speed peak to the north of the maximum surface wind speed. In the late afternoon, the marine layer was lower, and the potential temperature was up to 4 K warmer around 600 m over the northern end of the profile. This decrease in the marine layer depth through the day is consistent with the increased synoptic-scale subsidence noted in an earlier section.

5. Supercritical marine layer

To test whether the observed wind distribution might be due to supercritical flow effects, the Froude number
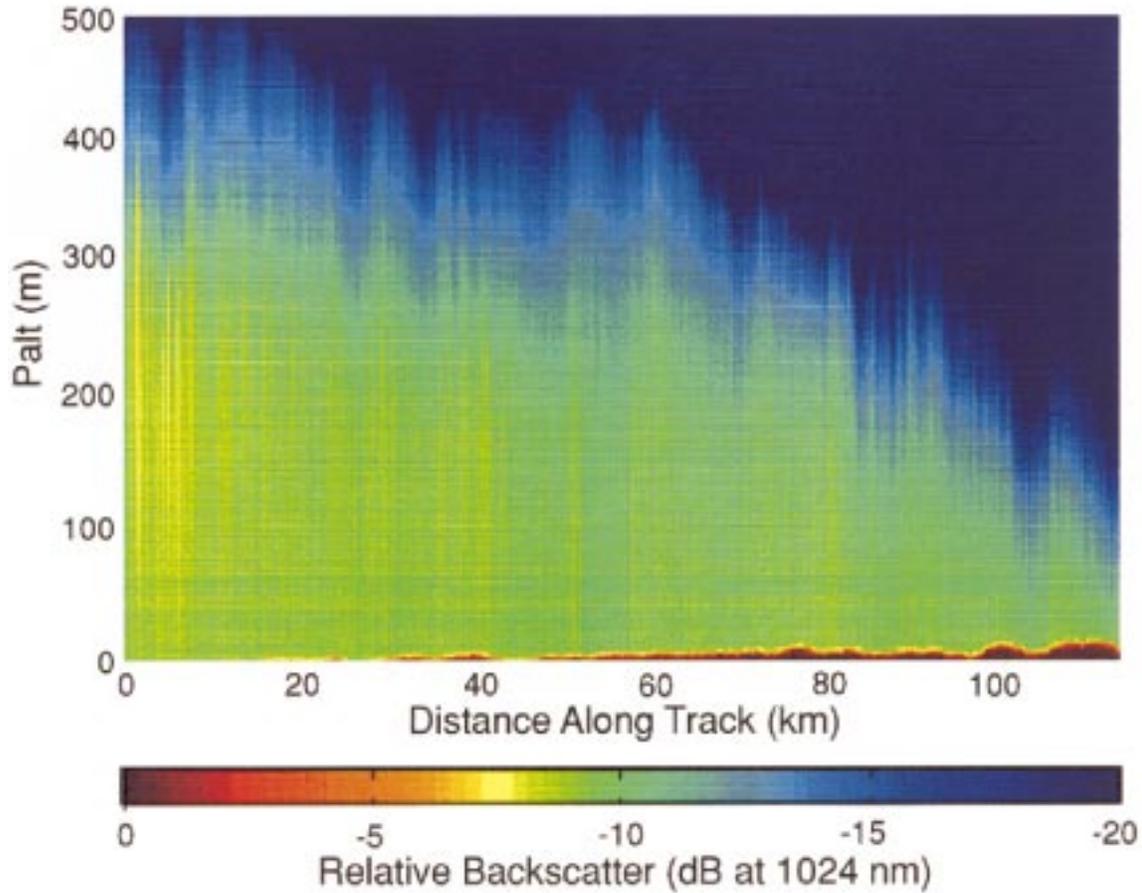
FIG. 7. Green, downward pointed lidar while flying at 900 m on the cross-coast midtrack corresponding to Figs. 6 and 11.

was calculated using the 47 aircraft soundings. Assuming that the flow may be considered as a single hydraulic layer capped by the air temperature inversion, the nature of the flow may be characterized by the Froude number that is based upon the the height of the air temperature inversion base and the potential temperature difference between the top and base of the air temperature inversion (Winant et al. 1988). As the air temperature inversion has a finite thickness, we shall expand the definition of the layer to include the lower half of the capping inversion layer and assume that the layer depth is thickness H, which is the average height of the air temperature inversion base and top. Then the Froude number is given by

$$\mathrm{Fr} = \frac{C}{\left[gH\dfrac{(\theta_u - \theta)}{\theta}\right]^{1/2}},$$

where θ is the potential temperature of the air temperature inversion base and θ_u is the potential temperature of the air temperature inversion top, g is gravity, and C is the mean speed from the sea surface to H (as defined above). The computed Froude numbers shown in Fig.

13 are nearly all between 1.0 and 2.0, which means that the layer is essentially supercritical over the entire area. The three lowest Froude numbers are 0.76, 0.95, and 0.99, which occur just north of Point Sur where there is wind speed minimum and a layer depth maximum. The highest is 2.8, which is in the coastal, high speed zone just south of Point Sur where the inversion base is the lowest and the winds are the fastest. It should be recalled that our definition of the layer depth includes the lower half of the capping inversion layer. If the depth of the layer were defined as the lower air temperature inversion base height (as is sometimes done), the Froude number would be greater, with average values being near 2.0 and the maximum greater than 4.0.

To further examine the dynamics of the marine layer, simple energy calculations may be done assuming simple, frictionless, Bernoulli dynamics (Ippen 1951; Winant et al. 1988). The kinetic energy of the layer is $\frac{1}{2}V^2$, where V is the mean speed over the layer, and the potential energy of the layer is given by $gH(\theta_u - \theta)/\theta$, where the variables are defined as above. The total energy, which is the sum of both, should be constant along a streamline. Three coast-parallel, sawtooth sounding tracks were selected as the soundings are along an ap-
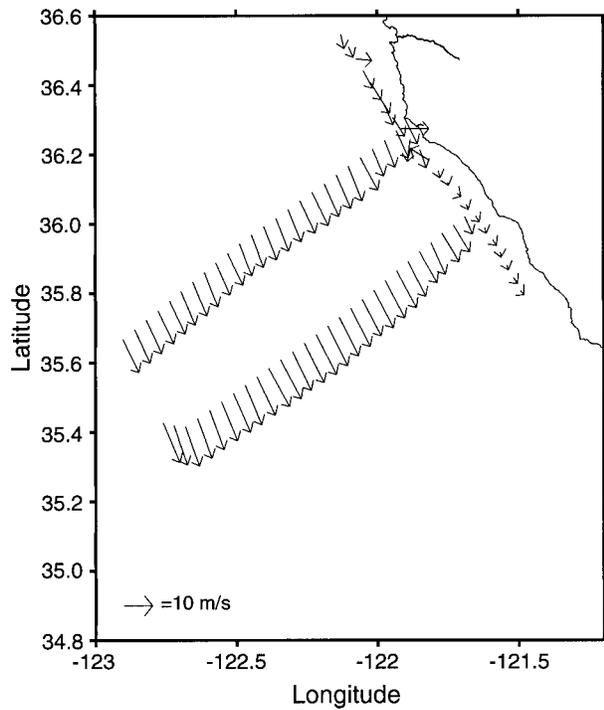
FIG. 8. Wind vectors at 900–1000-m elevation for 17 Jun 1996. Away from the immediate coast, wind direction is almost uniformly from 330° to 340°. Along the coast, speeds are weak and direction is more variable although they are also from the NNW and there is no significant cross-coast, offshore flow.
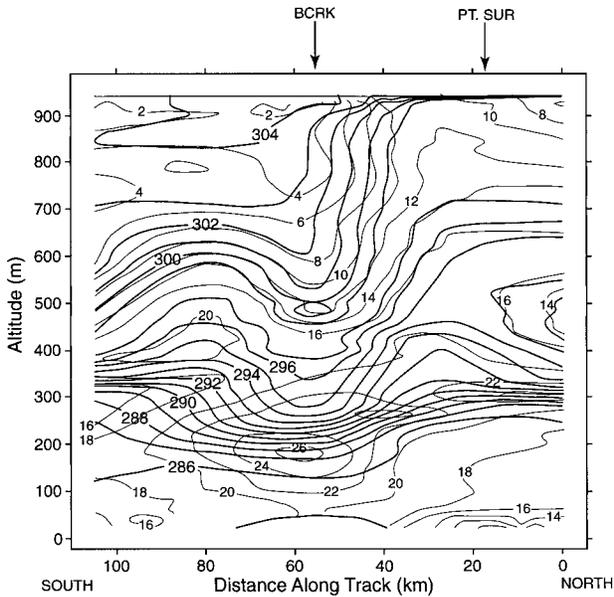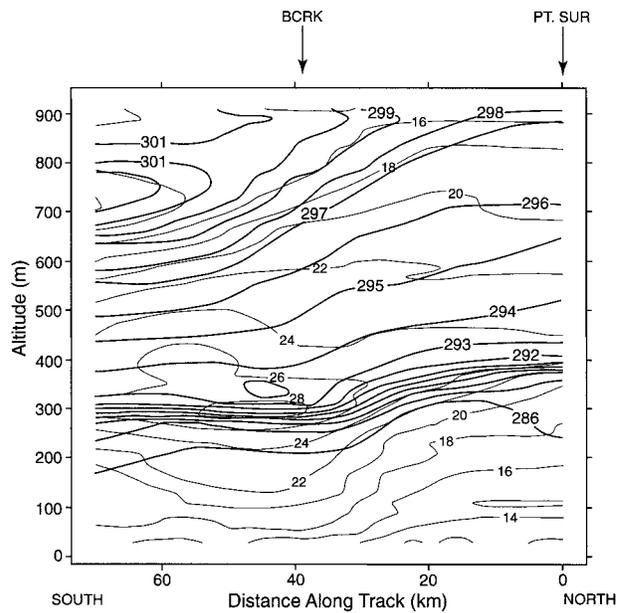

FIG. 10. Aircraft potential temperature (dark lines, K) and wind speed (light lines, m s^{-1}) for the alongcoast west profile.

proximate streamline the flow field should be relatively stationary over the 18-min flight time for each leg. Sounding locations are shown in Fig. 14, and calculations are shown for three coast-parallel tracks in Table 2. (The soundings A1 and A2 were not taken in the same track and time as the others on the east track. They will be discussed later.) The percent change refers to the change in energy from the northernmost sounding on that track. The northern two "S series" soundings on the east track, the northern three soundings on the middle track, and all of the west track have values in

FIG. 9. Aircraft potential temperature (dark lines, K) and wind speed (light lines, m s^{-1}) for the alongcoast east profile 3 made at end of flight.
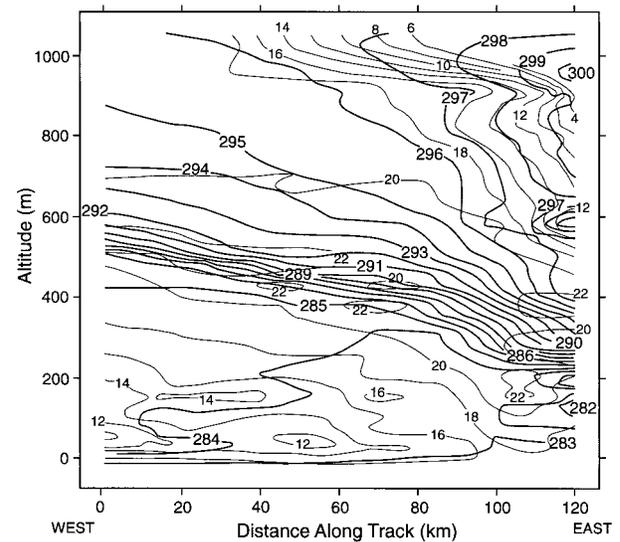

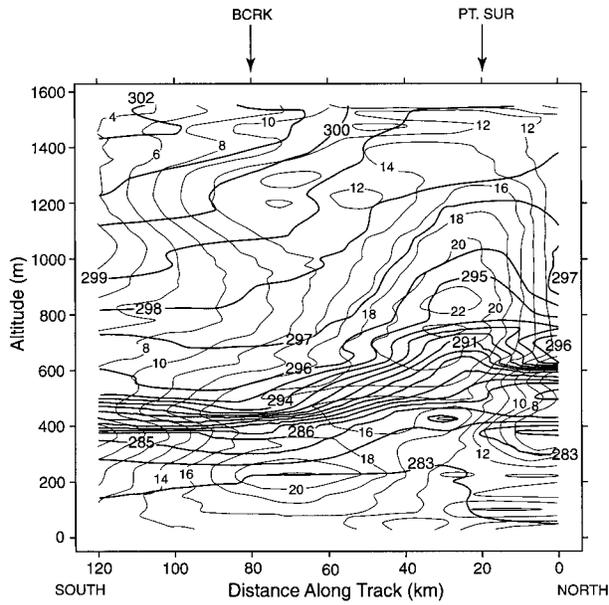FIG. 11. Aircraft potential temperature (dark lines, K) and wind speed (light lines, m s^{-1}) for the cross-coast midprofile.

FIG. 12. Aircraft potential temperature (dark lines, K) and wind speed (light lines, m s⁻¹) for the alongcoast east profile 1 made at start of flight on 17 Jun.
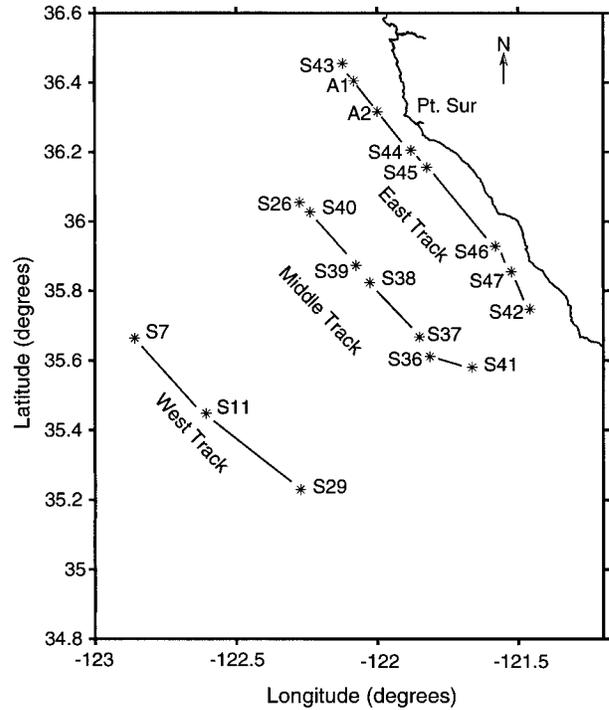

FIG. 14. Sounding locations used for layer energy calculations in Table 2. The "S" soundings on a track were all taken within 20 min as the aircraft flew a sawtoothed pattern from 30 m to above 900 m. The "A" soundings were taken hours earlier on different tracks but highlight the proposed oblique hydraulic jump feature discussed in the text.

the range of 252–327 m⁻² s⁻², while the energy along the central part of the east track and southern half of the central track is above 400 m⁻² s⁻². The increase in these above those on the north end of the tracks is largely due to the change in the potential temperature difference between the inversion base and top that increases by about one-third. If the potential temperature difference had remained the same along a track, the total energy would have decreased or remained the same along each track. Thus, horizontal changes in the thermal structure in the capping layer is modifying the energy of the marine layer in an expansion fan.

6. Numerical model

The COAMPS model, described in section 2, was run in support of the observational program. The model fields provide a larger-scale, spatially continuous, three-dimensional context in which to view the aircraft observations. Thus, the model fields are used as an aid in interpretation of the observations presented above.

The 9-km domain is shown in Fig. 15 along with the terrain height field and some geographical locations. The numerical simulation for the 24-h period beginning at 0000 UTC 17 June 1996 features strong northerly and generally coast-parallel flow in the marine atmo-
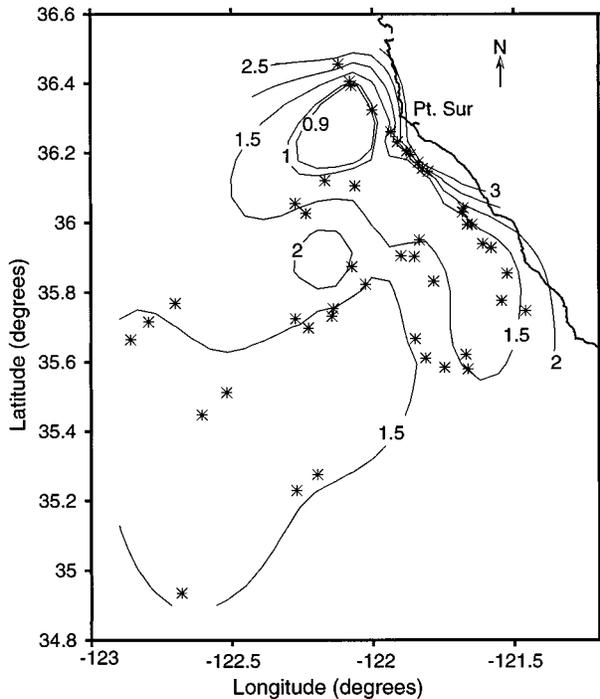

FIG. 13. Froude numbers for 17 Jun 1996. The marine layer in the area is almost completely supercritical with the greatest values in the lee of Point Sur close to the coast. The three subcritical soundings are on the north side of Point Sur, next to the coast, and are believed to be an oblique hydraulic jump.

TABLE 2. Track energy.

	West track energy			Middle track energy							East track energy							
	S29	S11	S7	S41	S36	S37	S38	S39	S40	S26	S42	S47	S46	S45	S44	A2	A1	S43
Spd (m s⁻¹)	18.4	17.2	17.3	22.5	21.8	23.1	21.9	19.7	17.2	17.7	20.9	17.8	19.1	22.5	21.3	12.9	11.9	21.6
Pot (K)	10.8	9.2	8.7	14.9	14.3	14.2	14.4	8.5	8.4	10.7	14.6	15.8	17.5	15.7	9.0	9.4	12.5	8.8
Ht (m)	451	513	536	471	396	438	461	334	357	462	337	354	400	312	266	528	568	307
Froude	1.42	1.35	1.37	1.45	1.56	1.58	1.45	1.99	1.69	1.35	1.60	1.28	1.23	1.73	2.34	0.99	0.76	2.24
KE (kg m² s⁻²)	170	149	150	253	238	268	240	194	148	156	219	158	182	254	227	83	71	233
PE (kg m² s⁻²)	168	163	161	242	196	215	229	98	104	171	170	193	242	169	83	171	245	93
TE (kg m² s⁻²)	338	312	311	495	434	483	469	292	252	327	389	351	424	423	310	254	316	326
% change	+9	+0	ref	+52	+33	+48	+44	−11	−23	ref	+19	+8	+30	+30	−5	−22	−3	ref

KE = kinetic energy; PE = potential energy; TE = total energy; POT = potential energy difference between inversion top and base.
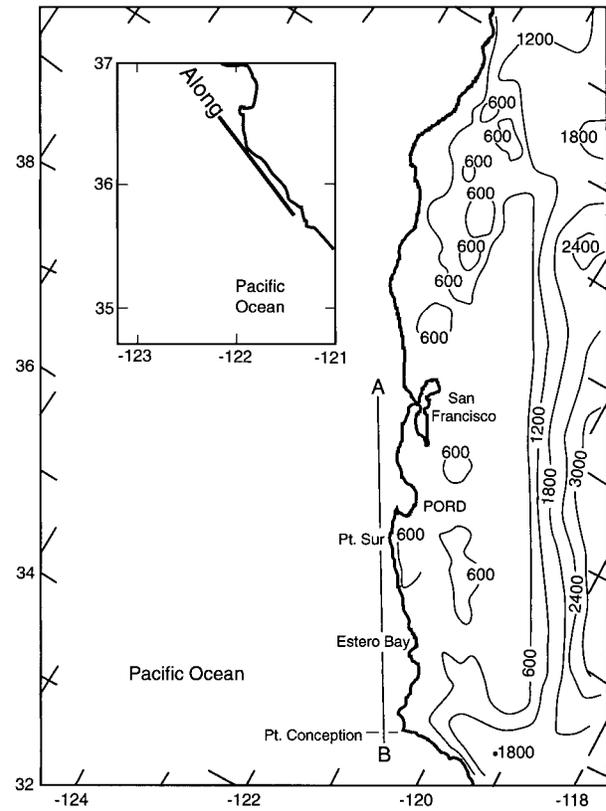

FIG. 15. Map showing COAMPS model domain and locations referenced in text.

spheric boundary layer (MABL) with significant acceleration in the lee of Point Sur. A typical example is shown in Fig. 16, which is the 21-h forecast 10-m level wind vectors and isotachs valid at 2100 UTC 17 June over a subsection of the model domain extending from just north of San Francisco Bay to Estero Bay and out to 180 km offshore. This figure compares favorably with Fig. 3; note that the model wind speeds are consistent with the observed wind speeds adjusted to the 10-m level, and the wind direction from the model corresponds well with the observations, including the larger northerly component north of Point Sur and the larger westerly component to the south. Further examination of the model output indicates that the maximum wind speed in this region increased from 12 m s⁻¹ at 1200 UTC 17 June (not shown) to 17 m s⁻¹ at 0000 UTC 18 June. These temporal changes are consistent with the general increase in near-surface wind speed over the flight time of the aircraft noted above in section 4d.

Figure 17 shows a model cross section extending from just south of Point Conception to just north of Point Año Nuevo and from the surface to ~1500 m. The forecast cross section at 2100 UTC shows, moving southward from the north end, the MABL rises and speeds decrease to just north of Point Sur, then strong acceleration (from 18 to 24 m s⁻¹) and suppression of
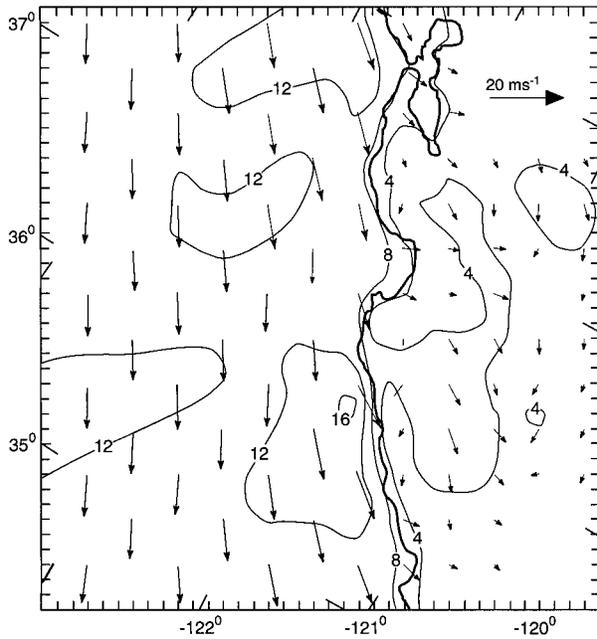
FIG. 16. COAMPS model wind vectors and isotachs (m s^{-1}) at the 10-m level at 2100 UTC 17 Jun 1996.

FIG. 17. COAMPS cross section of potential temperature (dark lines, K) and wind speed (light lines, m s^{-1}) at 2100 UTC. The plane of the cross section (AB) is shown in Fig. 15. The response to Point Sur extends throughout the marine layer and the inversion layer above.

the MABL in the lee of Point Sur. The core of the high wind speed lies at the base of the inversion. Above the MABL, isotherms sink to a minimum in the lee of Point Sur while speeds decrease sharply. Between 1800 and 0000 UTC, the inversion strengthens and the base height lowers over the entire plane of the cross section, consistent with the synoptic-scale evolution noted earlier and time series at the NPS profiler site.

The model MABL wind speed and depth were used to estimate the layer Froude numbers. Froude numbers were computed using Fr $= C(Nh)^{-1}$, where C is the total wind speed, N is the stabilitiy, and h is the depth of the mixed layer. The model indicates that the flow everywhere in the vicinity of the central coast is supercritical, including that on the inbound, north side of Point Sur. Model Froude numbers range from a high of 3.2 near Point Sur to 1.3 near Point Conception, which are comparable to aircraft sounding-based values of a high of 2.8 near Point Sur and 1.5 to the south (Fig. 13).

To show the degree that the larger-scale model fields mesh with the aircraft-measured fields, and how well the model expresses the structural changes across Point Sur, one alongcoast cross section is presented that matches an aircraft vertical section. In Fig. 18 is a cross section of potential temperature and wind speed derived from the model 18-h forecast fields valid at 1800 UTC 17 June in a plane to approximately match the time and position of the aircraft cross section designated in the along coast east profile 1 (Fig. 12). Examination of these figures shows that the model has captured all of the significant features in the observations. In terms of po-
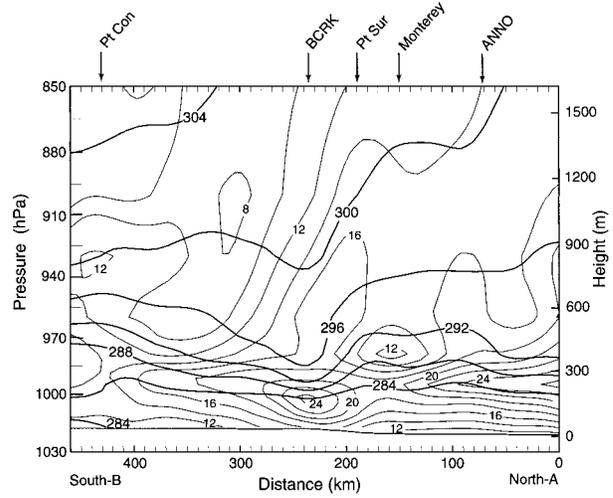
tential temperature, the abrupt decrease in boundary layer depth near the center of the track, the significant increase in inversion strength to the south, and the general slope of the isentropes from north to south are present in both the model and observations. The model underforecast the depth of the MABL, which ranges from ~160 m in the south to over 300 in the north, as compared to 200–400 m in the aircraft observations. In terms of the wind speed, the isotach maximum sloping downward from north to south is depicted in model output. The wind speed maximum is slightly underforecast (19 m s^{-1} in the model vs 21 m s^{-1} in the observations).

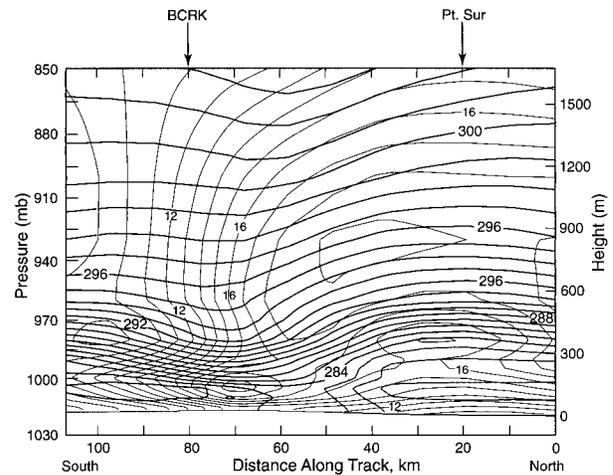Other aspects were compared between the model and

FIG. 18. COAMPS cross section for 1800 UTC 17 Jun 1986. This section matches the approximate position and time of the aircraft cross section alongcoast east profile 1 (Fig. 12).
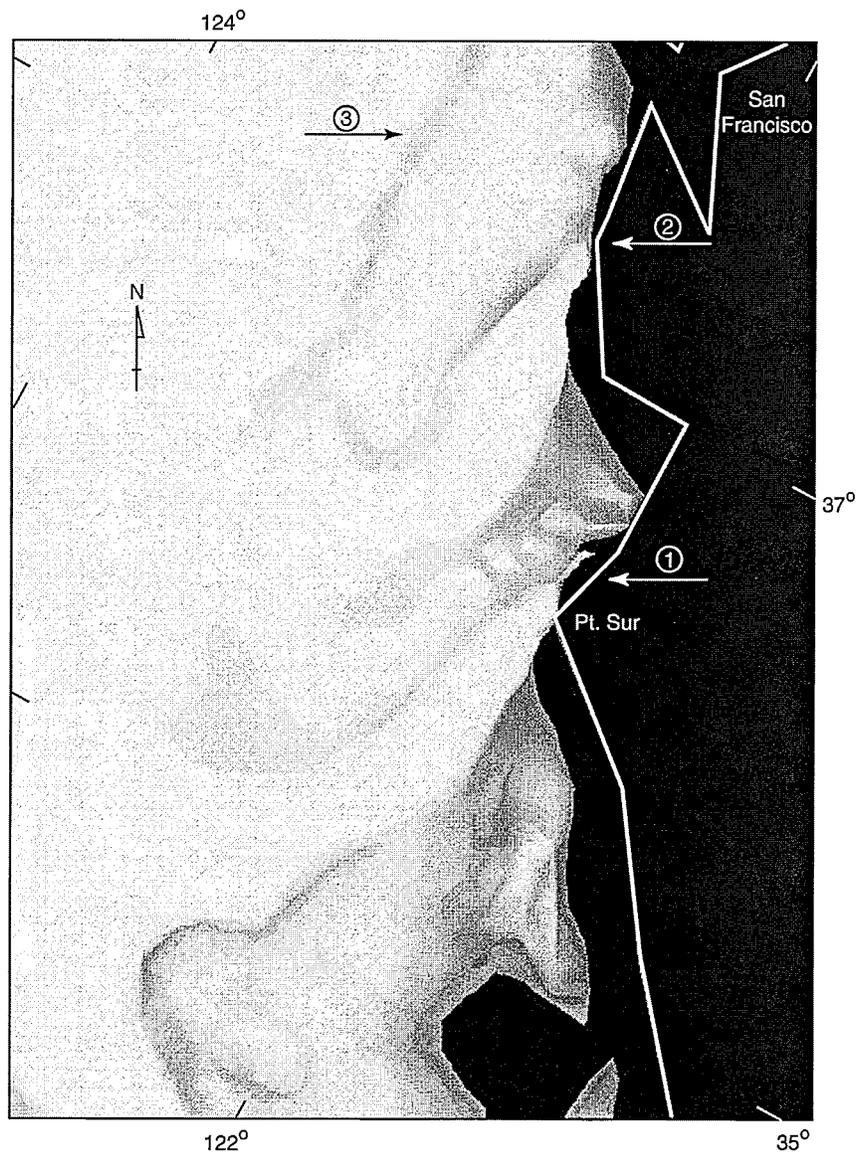
FIG. 19. Three-dimensional rendering of the COAMPS 286-K isentropic surface valid at 0000 UTC 18 Jun l996. There is a valley in the surface that extends west from Monterey Bay while the surface extends to the sea surface in the lee of Point Sur. Between is a steep ridge with a finger extending over land to the formation point on the upwind side of the topography behind Point Sur (lower arrow). Similar but less dramatic shocklike features extending from other costal bends are noted by the other arrows, with the uppermost extending from Point Arena, which is off the map.

the aircraft observations. The sea level pressure field (not shown) is also in good agreement with the larger-scale aspects of the observation (Fig. 3), although the intense, small-scale pressure gradients near the coast in the lee of Point Sur are not depicted in the model. Above the marine boundary layer (at ~1 km) the model indicates an offshore component in the lee of the high terrain near Point Sur that is not present in the aircraft observations. The overall conclusion based upon these sections and others not shown is that the moderate scale aspects of the model agree well with the observations.

Aircraft data indicates a hydraulic jump–like feature just north of Point Sur and close to the coast. In order to more fully characterize the three-dimensional structure, a three-dimensional rendering of the model output was constructed to look for structure on the north side of Point Sur. Shown in Fig. 19 is a view downward onto the 286-K isentropic surface at 0000 UTC 18 June. This temperature was selected as it is near the center of the inversion capping the MABL for most of the area in this study. This surface is constructed such that everywhere above this surface is warmer (in potential tem-

perature) than 286 K. The blue region on the east side is open ocean where the sea level surface potential temperature is greater than 286 K. Thus, the yellow surface gives a rather striking depiction of the topography of the inversion. Note the deep depression in the surface extending to the southwest from Monterey Bay and another just to the south of Point Sur. Smaller depressions extend from the point just north of Pigeon Point (upper-right arrow) and Point Arena (upper left arrow), which is out of view although the depression extends into the northern, central edge of the analysis. These depressions show the regions in which the boundary layer is suppressed due to presumed expansion fans downwind of points along the coast. Note also the narrow finger of the 286-K surface pointing at Point Sur that is formed by the extremely sharp boundary between the depressions extending from Point Santa Cruz and Point Sur (lower arrow). This feature is due to interaction of the supercritical marine layer with the topography near Point Sur and is believed to an oblique hydraulic jump that will be discussed in the next section. The middle arrow points to a smaller finger of a compression feature on the north side of Pigeon Point. Thus, the three-dimensional rendering allows visualization of the mesoscale features, which are the subject of this paper as well as showing the relationship between the event sampled by the aircraft and related phenomena elsewhere along the coast.

7. Discussion

Direct aircraft measurements show, and modeling confirms, that the marine boundary layer was supercritical along central California on 17 June 1996. COAMPS modeling indicates that the supercritical MABL extended well beyond the aircraft mapped area both to the north and south of Point Sur. Closer to Point Sur, aircraft soundings indicate that the MABL was weakly supercritical with the Froude numbers mostly in the range of 1–2 with 2.8 the highest using the elevation halfway between the air temperature inversion base and top as the layer thickness. This is a lower bound on the Froude number, as less restrictive computations using the inversion-base elevation for the layer thickness would generally increase the Froude numbers by about 25%, which would not substantially change the characterization.

The measured structure, supported by the model, is strongly suggestive of an inbound supercritical MABL interacting with the topographic bend in the coast at Point Sur, forming a supercritical expansion fan in the lee. Calculating the linear shock characteristics associated with the expansion fan is of marginal use for a three-dimensional flow case where it is very subjective to select the inbound values. In the lee of Point Sur, the computed value might be around 30°–40° (Ippen 1951) whereas one might pick out something around 38° from the aircraft mapping flights (Fig. 3).

The three-dimensional structure of the marine layer and speed is more complex than that of a simple linear layer where characteristics extend infinitely outward from the coast (Ippen 1951; Winant et al. 1988). Instead, the inbound supercritical becomes more supercritical in the lee within localized zones of a wind speed maximum and layer depth minimum centered in the lee of the obstacle. This conforms closely with the layer structure of, and is a confirmation of, Samelson's (1992) model of a supercritical expansion fan at a coastal bend for single layer with rotation and friction.

In the observations, some features were found that suggest unanticipated complexity beyond the successful but simple model with rotation and friction as suggested by Samelson (1992). One is a narrow, weak wind speed zone adjacent to the straight section of coast downwind of Point Sur. Weak winds and moist, cool marine are measured at the BCRK surface station. The narrowness of the weak wind zone is confirmed by local inhabitants who regularly experience weak winds at the coast while at the same time seeing high wind produced ocean white caps a few kilometers offshore.

Another complexity is the layer energy along an approximate streamline was not constant, but increased in the southern half of the middle and east tracks. Most of this may be accounted for by the hotter air temperatures in the inversion, which increased the density difference across the top and the potential energy of the layer. A more horizontally uniform temperature field in the inversion would yield better energy conservation. As shown in Fig. 16, COAMPS confirms that deep subsiding air above the marine layer in the vicinity of Point Sur is associated with this, and the warming is more than just that which would occur due to changes of the air temperature inversion base height.

Between Monterey and Point Sur, there is a hydraulic jump–like feature on the inshore leg (Fig. 4). This is consistent with an oblique hydraulic jump forming on the upwind side on the outward coastal projection of the Point Sur area (Chow 1959). A supercritical layer impinging upon an outward bend in a confining wall will have a step increase in layer depth and a step decrease in layer speed. Fast surface winds were measured by the aircraft for the first 7 km of the north end of the along coast east track 3 followed by a rapid decrease in wind speed (Fig. 4). The step change is a shock characteristic that will extend away from the wall and downstream of the corner. Simple linear theory forecasts a turn of a few degrees away from the corner although a 15° shift was observed in the wind direction on the adjusted, 10-m leg (Fig. 4). Coincident with a rapid drop in speed is a 1-hPa increase in pressure. By hydrostatics, a 1-hPa surface pressure increase would correspond to a 200-m increase in the inversion temperature base height (Dorman 1985), which is close to what was found by the aircraft soundings (Fig. 3c) and the lidar (Fig. 5). The lidar on the alongshore track 3 (Fig. 5) shows the low marine layer suddenly deepening over less than

2 km followed by at least five wavelike crests in height. The step change and waves are structurally similar to an undular hydraulic jump typical for Froude numbers of 1–1.7 (Chow 1959), which is also in the range of the aircraft-measured Froude number on the upwind side (Fig. 13). The northernmost sounding (S43) had a shallower and faster marine layer than two soundings just to the south (A1 and A2, Table 2). The total energy in A2 is less than A1 or S43, which is consistant with a loss in a hydraulic jump. However, the conclusions about the soundings are somewhat weakened by the A1 and A2 soundings being taken hours earlier than S43 and the fact that the soundings were taken on a long slant path of the order 10 km that marginally resolved this feature. Finally, the 286-K isentropic surface generated by COAMPS forecast a steep-sided, narrow feature originating on the upwind side of the steep topography behind Point Sur while extending offshore and downwind that has the aspect of a shock characteristic of an oblique hydraulic jump. These observations and model results support an oblique hydraulic jump on the north side of Point Sur.

8. Conclusions

Aircraft soundings show that the marine boundary layer was supercritical in the area from 40 km north of Point Sur to 60 km south of Point Sur, and 120 km offshore on 17 June 1996 with the exception of one small area close to the coast and on the upwind side of Point Sur. Froude numbers were mostly in the range of 1.0–2.0. The COAMPS model is consistent with the aircraft-measured 10-m wind speeds, boundary layer depths, and supercritical conditions extending over the central California coastal waters well beyond Point Sur. The northerly flow produced a marine boundary layer structure highly consistent with a supercritical expansion fan in the lee of Point Sur. This confirms Samelson's (1992) model of a single layer with rotation and friction interacting with a convex coastal wall.

Aircraft measurements indicate an oblique hydraulic jump feature close to the coast on the north side of Point Sur. The COAMPS model forecast a narrow, sharp jump in height of isotherms in the inversion forming on the upwind side of Point Sur and extending offshore and downwind as a shock characteristic. The combination of these observations supports the existence of the northerly, supercritical marine layer initiating an oblique jump on the upwind side of the elevated topography behind Point Sur.

REFERENCES

Beardsley, R. C., C. E. Dorman, C. A. Friehe, L. K. Rosenfeld, and C. D. Winant, 1987: Local atmospheric forcing during the coastal ocean dynamics experiment. I. A description of the marine boundary layer and atmospheric conditions over a northern California upwelling region. *J. Geophys. Res.,* **92,** 1467–1488.

Chow, V. T., 1959: *Open-Channel Hydraulics.* McGraw-Hill, 680 pp.

Dorman, C. E., 1985: Evidence of Kelvin waves in California's marine layer and related eddy generation. *Mon. Wea. Rev.,* **113,** 827–839.

——, 1987: Possible role of gravity currents in northern California's coastal summer wind reversals. *J. Geophys. Res.,* **92,** 1497–1506.

——, and C. D. Winant, 1995: Buoy observations of the atmosphere along the west coast of the United States, 1981–1990. *J. Geophys. Res.,* **100,** 16 029–16 044.

Hodur, R. M., 1997: The U.S. Navy's Coupled Ocean/Atmosphere Model (COAMPS). *Mon. Wea. Rev.* **125,** 1414–1430.

Ippen, A. T., 1951: Mechanics of supercritical flow. *Trans. Amer. Soc. Civil Eng.,* **116,** 268–295.

Large, W. G., and S. Pond, 1981: Open ocean momentum flux measurements in moderate to strong winds. *J. Phys. Oceanogr.,* **11,** 324–481.

Neiburger, M., D. S. Johnson, and C. Chien, 1961: Studies of the structure of the atmosphere over the eastern Pacific Ocean in Summer, I, The inversion over the eastern North Pacific Ocean. *Univ. Calif. Publ. Meteor.,* **1,** 1–94.

Nelson, C. S., 1977: Wind stress curl over the California current. NOAA Tech. Rep. NMFS SSRF-714, 87 pp. [NTIS PB-273-610/6GI.]

Paulson, C. A., and J. J. Simpson, 1981: The temperature difference across the cool skin of the ocean. *J. Geophys. Res.,* **86,** 11 044–11 054.

Samelson, R. M., 1992: Supercritical marine-layer flow along a smoothly varying coastline. *J. Atmos. Sci.,* **49,** 1571–1584.

Thompson, W. T., T. Haack, J. D. Doyle, and S. D. Burk, 1997: A nonhydrostatic mesoscale simulation of the 10–11 June 1994 coastally trapped wind reversal. *Mon. Wea. Rev.,* **125,** 3211–3230.

Winant, C., C. Dorman, C. Friehe, and R. Beardsley, 1988: The marine layer off northern California: An example of supercritical channel flow. *J. Atmos. Sci.,* **45,** 3588–3605.